Development of a unified design buckling curve for fibre reinforced polymer plates subjected to in-plane uniaxial and uniform compression

Downloaded from: https://research.chalmers.se, 2025-12-04 22:39 UTC

Citation for the original published paper (version of record):

Olsson, E., Mottram, J., al-Emrani, M. et al (2023). Development of a unified design buckling curve for fibre reinforced polymer plates subjected to
in-plane uniaxial and uniform compression. Thin-Walled Structures, 183.
http://dx.doi.org/10.1016/j.tws.2022.110346

N.B. When citing this work, cite the original published paper.

research.chalmers.se offers the possibility of retrieving research publications produced at Chalmers University of Technology. It covers all kind of research output: articles, dissertations, conference papers, reports etc. since 2004. research.chalmers.se is administrated and maintained by Chalmers Library

(article starts on next page)

Thin-Walled Structures 183 (2023) 110346

Contents lists available at ScienceDirect

Thin-Walled Structures

journal homepage: www.elsevier.com/locate/tws

Full length article

Development of a unified design buckling curve for fibre reinforced polymer plates subjected to in-plane uniaxial and uniform compression

Erik Olsson [a], J. Toby Mottram [b], Mohammad Al-Emrani [a], Reza Haghani [a,*]

[a] Department of Architecture and Civil Engineering, Chalmers University of Technology, Sven Hultins gata 6, 41296, Gothenburg, Sweden
[b] School of Engineering, The University of Warwick, Coventry, CV4 7AL, UK

ARTICLE INFO

Keywords:
Fibre reinforced polymer (FRP)
Plate
In-plane compression
Finite element analysis
Buckling
Post-buckling

ABSTRACT

Presented are 24 non-dimensional buckling curves to estimate the strengths of Fibre-Reinforced Polymer (FRP) square plates having four simply supported edges and subjected to in-plane uniaxial and uniform in-plane compression. The curves are constructed by the authors from a parametric numerical analysis using ABAQUS® software with changing variables for: material properties; initial geometrical imperfections; laminate lay-ups; and plate thicknesses. These strength curves express relationships for the buckling reduction factor with plate slenderness, and account for post-buckling strength. We observe that regardless of the laminate lay-up (except for purely unidirectional), the choice of FRP material and the magnitude of the initial geometrical imperfection the predicted buckling reduction factors display a meaningful correlation with plate slenderness. Presented is a proposed unified buckling design curve, defined as the lower bound to 18 of the 24 ABAQUS®-generated buckling curves. This new curve is benchmarked by the authors against experimental test results extracted from the literature and it is found that there is a reasonable agreement. The authors recommend that the proposed buckling design curve has the potential to be introduced into structural design standards as a procedure to design the buckling strengths of FRP plates.

1. Introduction

Fibre-Reinforced Polymer (FRP) composites in the form of thin-walled laminated structures are widely utilized around the world in different engineering applications. Their outstanding specific strengths and stiffnesses, fatigue endurance, corrosion resistance and lightweight characteristics have made them attractive structural materials in marine and aerospace sectors. Desirable mechanical properties, decreasing project costs [1], improved durability [2], sustainability credentials [3] and possibilities for prefabrication [4] have also made FRPs a structural material of choice for applications in civil engineering works. Among other application areas, transport infrastructure such as bridges [5–9], tunnel linings [10], underground culverts [11] and sheet piles [12] has taken advantage of FRP composites being a viable type of construction material. Due to increasing interest in the application of FRPs in the construction sector, Work Group 4 *Fibre Reinforced Polymer Structures* entrusted to CEN/TC 250 (the CEN Technical Committee responsible for the suite of structural Eurocodes) has prepared the Technical Specification document *Design of Fibre-Polymer Composite Structures* (CEN/TS 19101:2022) [13], which is to be the basis for the future Eurocode with the same scope and content.

New-build FRP structures are constructed of thin-walled elements [8], and it is acknowledged that their structural design is often governed by excessive deformations [14] or instabilities (i.e., mechanism of buckling) [15]. The basic building blocks of these structural elements is laminated plates. Theoretical perfectly flat laminated plates of FRP materials subjected to in-plane compression loads will firstly respond with in-plane displacements only, but when the compression stress is high enough, out-of-plane displacements occur. Plate buckling is the latter of these structural responses being characterized in terms of critical load and out-of-plane deformations. At the elastic critical buckling load, these deformations can become excessive. In classical buckling theory, the compression load vs. out-of-plane displacement curve shows a bifurcation behaviour at this critical load, at which the plate response is distinctly different before and after; with only in-plane deformations immediately before and with 'excessive' out-of-plane deformations immediately after. Elastic critical buckling loads for laminated plates can be predicted using the classical buckling theory of first-order that is derived using the Kirchhoff hypothesis, stating "Normal to the mid-plane remain straight and normal as the plane deforms into a surface" [16]. The response of plates and their strengths for loading above their critical buckling loads is the focus of this contribution to knowledge and understanding. We consider the post-buckling response of compressed plates during which they can resist further compressive stress before experiencing ultimate failure by FRP material fracture.

* Corresponding author.
E-mail address: reza.haghani@chalmers.se (R. Haghani).

https://doi.org/10.1016/j.tws.2022.110346
Received 30 July 2022; Received in revised form 12 September 2022; Accepted 3 November 2022
Available online xxxx
0263-8231/© 2022 The Author(s). Published by Elsevier Ltd. This is an open access article under the CC BY license (http://creativecommons.org/licenses/by/4.0/).

Technical Specification (CEN/TS 19101:2022) [13] recommends in Section 8 using the elastic critical buckling loads (as stresses) for a representative measure for the ultimate strength of laminated plates, and thereby as the basis for design values. While considering elastic critical buckling loads is straightforward, for FRP plates with intermediate slenderness it will result in conservative strength estimations, mainly because the first-order approach neglects the post-buckling reserve strength [17,18]. Moreover, according to the study reported herein, it may result in unsafe design strengths for plates having relatively low slenderness. Furthermore, elastic critical buckling loads would normally not be enough for design and the procedure needs separate checks for material failure using appropriate failure criteria [19]. To reliably predict the load capacity of compressed FRP plates, the ultimate strength analysis must account for material stiffness degradation associated with post-buckling deformations and ply failures. In addition, test results do show that rectangular plates subjected to in-plane uniform and uniaxial compression can experience a significant influence on load-carrying capacity in the presence of initial geometrical imperfections [20], underlining the importance in stress analysis studies of this inherent and uncertain physical variable.

Buckling stress analysis of rectangular FRP laminated plates, with various displacement and in-plane loading boundary conditions, has been the subject of numerous analytical and numerical studies since the 1960s. Early studies for this important subject are limited to determining the critical elastic buckling loads of perfectly flat plates subjected to in-plane uniaxial compression or shear, having different displacement and stress boundary conditions. It is notable that several analytical and numerical solutions have been proposed and for an introduction to these outcomes six references are given [21–26]. There is also a significant amount of research devoted to studying the post-buckling behaviour of compressed slender plates, specifically of FRP laminates [27–31], where both analytical and numerical methods are employed to predict the instability onset and post-buckling loads. When practical to do so, the predictive performance has been evaluated by comparing with experimental test results. The effects on buckling behaviour of the presence of initial geometrical imperfections in the FRP plates have been included, see for example Refs. [21,31].

From a literature review we observe that less attention has been paid to formulating the post-buckling reserve strength and to using this data to construct and recommend a proposed design approach for the buckling strength of compressed FRP plates. This finding we attribute to two facts, which are that:

1. to achieve realistic numerical predictions, global damage models, such as ply elimination upon detection of ply-level failure should be avoided and instead localized progressive damage models at the ply-level need to be used.
2. the product-based-design approach and popularity of design by testing [5] in aerospace, marine and transportation sectors are reasons for a barrier to developing a unified design approach based solely on numerical results.

It is noted that for the application of models to satisfy 1 it is necessary to use advanced numerical methods and considerable computing resources. We observe that advanced finite element software may not be time- and cost-effective to structural engineering practitioners for the design of civil engineering works, and so they desire to conduct supportive design checks in accordance with structural design standards, such as the Eurocode part under preparation (see CEN/TS 19101:2022 [13]). This background knowledge supports the need for the development of easy-to-use, yet dependable, design procedures to scope the ultimate limit state failure of FRP laminated plates when the initial mode of failure is due to buckling, followed by material failure.

In this paper, the authors present such a design procedure in the form of a non-dimensional unified buckling curve. In this contribution the scope of the proposed strength curve is for square plates with symmetric, balanced FRP laminates (not with unidirectional reinforcement) subjected to in-plane uniform and uniaxial compression load and having simply supported boundary conditions along the four sides. Importantly, the numerical predictions used to construct the curves account for both the post-buckling reserves of strength and the reductions of strength owing to initial geometrical imperfections. Moreover, employing finite element analysis for determining post-buckling responses will inherently include the effect of shear deformation.

2. Numerical analysis and the finite element modelling

2.1. Material properties and plate variables

To commence the numerical parametric study, it is first necessary to define a restricted, yet effective range of variables for the plate dimensions and the FRP materials. Modelled is a square plate having side lengths of 500 mm of different laminations of either E-glass epoxy or T300 carbon epoxy. For these two FRP materials the matrix is always of the epoxy resin Fiberite 934. Presented in Table 1 are the assumed material properties taken from [32] for the individual plies having a unidirectional reinforcement of carbon or glass fibres. Column (1) in the table gives the 12 material properties with their notation. In column (2) are the units and the property values are in columns (3) and (4). It is assumed for constitutive modelling in the finite element simulations that there is a linear elastic relationship between stress and strain up to the point of the ultimate failure of the unidirectional materials.

When the continuously aligned fibres in a ply are aligned with the principal direction in the laminate the direction of these fibres is 0-degrees, which is the direction in which the compression load for the buckling instability is applied. Plies are oriented at 90-degrees when fibres are aligned perpendicular to the laminate's principal direction. Next, we specify the laminates used in the study. Listed in Table 2 are four lay-ups, with column (1) defining these to be: unidirectional (hereafter abbreviated to UD); 0-dominated; 45-dominated; quasi-isotropic. Each lay-up is associated with a lamination code that is defined in column (2), where x is to be replaced by the numbers in column (3). x is either the number of plies or repetitions of a group of plies, for UD, 0-dominated and quasi-isotropic lay-ups, has six different integers, resulting in laminates with six different total number of plies or thicknesses. For the numerical study Table 2 defines a total of 26 unique laminate lay-ups. With a constant thickness of 0.6 mm assumed for each ply. Table 3 lists that there are eight different thicknesses with column (1) listing their code numbers. Thickness code numbers 7 and 8 are only relevant to the 45-dominated lay-ups and represent the 12 and 20-ply laminates, as indicated by the asterisks in Table 3. Column (2) in Table 3 gives the number of constant thickness plies and the laminates' thicknesses are listed in column (3). The variation in thickness of the plates is seen to be from 4.8 mm (for 8 plies) to 28.8 mm (for 48 plies); note that the side dimensions of the square plate are fixed at 500 mm.

The final variable to be specified is for a plate's out-of-plane geometrical imperfection. Table 4 reports the three magnitudes for this initial imperfection. Column (1) lists the magnitudes as a ratio of the side dimension b (equal to 500 mm) and column (2) gives them in terms of out-of-plane displacements as 0.05, 2.5 and 5 mm. The smallest at 0.05 mm is assumed to represent an almost perfectly manufactured laminate (500 by 500 mm), whilst magnitudes of 2.5 and 5 mm are taken to represent 'medium' to 'large' imperfections. This range in magnitudes is justified by previous numerical studies conducted by Fallah *et al.* [20] and Hayman *et al.* [33].

Every numerical model is allocated a unique label of the format *X_Y_Z_T*, as introduced by the information presented in Table 5. Column (1) lists the four components in the labelling scheme with columns (2) and (3) for the variables' notations and their descriptions, respectively. For example, label **G_0_10,000_3** is for the model consisting of: E-**G**lass-epoxy plies (X); **0**-dominated lay-up (Y), imperfection b/**10,000** (0.01%) or 0.05 mm (Z); thickness code **3** (for 14.4 mm) (T).

Table 1
Material properties for a ply of unidirectional E-glass epoxy and a unidirectional T300 carbon epoxy [32].

Material property	Unit	E-glass epoxy	Carbon epoxy
(1)	(2)	(3)	(4)
Fibre volume fraction	-	0.45	0.60
Longitudinal modulus, E_{11}	GPa	38.6	148
Transversal modulus, E_{22}	GPa	8.27	9.65
Major Poisson's ratio, ν_{12}	–	0.26	0.30
In-plane shear modulus, G_{12}	GPa	4.14	4.55
Transverse shear modulus, G_{13}	GPa	4.14	4.55
Transverse shear modulus, G_{23}	GPa	4.14	4.55
Longitudinal tensile strength, X^{T}	MPa	1062	1314
Longitudinal compressive strength, X^{C}	MPa	610	1220
Transverse tensile strength, Y^{T}	MPa	31	43
Transverse compressive strength, Y^{C}	MPa	118	168
In-plane shear strength, S^{LT}	MPa	72	48

Table 2
Lay-ups and their unique laminate code (variable x in column (2) is replaced by the numbers in column (3)).

Lay-up	Laminate code	Value of x
(1)	(2)	(3)
Unidirectional (UD)	$[0_x]_s$	4, 8, 12, 16, 20, 24
0-dominated	$[90/\pm45/0_x]_s$	1, 5, 9, 13, 17, 21
45-dominated	$[90/\pm45_x/0]_s$	1, 2, 3, 4, 5, 7, 9, 11
Quasi-isotropic	$[[90/\pm45/0]_x]_s$	1, 2, 3, 4, 5, 6

Table 3
Different number of plies and plate thicknesses.

Thickness code	Number of plies	Plate thickness [mm]
(1)	(2)	(3)
1	8	4.8
2	16	9.6
3	24	14.4
4	32	19.2
5	40	24
6	48	28.8
7	12[a]	7.2
8	20[a]	12.0

[a]Only used for 45-dominated FRP plates (for x = 2 and 4).

Table 4
Three different initial imperfections based on the plate width of 500 mm.

Initial imperfection (% of plate sides)	[mm]
(1)	(2)
b/10000 (0.01%)	0.05
b/200 (0.5%)	2.5
b/100 (1%)	5

Table 5
Description for plate labelling X_Y_Z_T.

Component	Variable's notation	Description
(1)	(2)	(3)
X	G	E-glass-epoxy material
	C	Carbon-epoxy material
Y	UD	Unidirectional lay-up
	0	0-dominated lay-up
	45	±45-dominated lay-up
	Q	Quasi-isotropic lay-up
Z	10000	Imperfection b/10000
	200	Imperfection b/200
	100	Imperfection b/100
T	1–6 or 1–8	Thickness 4.8 to 28.8 mm (*c.f.* Table 3)

2.2. Finite element modelling methodology

In what follows the authors present the finite element modelling methodology that they adopted to achieve reliable and relevant predictions of buckling strengths using the variables defined in Section 2.1. To conduct the numerical study we used the commercial software package ABAQUS® 2017 [34]. As specified in Section 2.1 square laminated plates, with simply supported displacement boundary conditions, having side dimension 500 mm are subjected to uniform uniaxial and in-plane compression in the 0° direction for the lay-ups in Table 2. The mesh is comprised of quadratic eight-node elements (type S8R) possessing reduced integration and with six degrees of freedom at each node. The plate volume is modelled as a deformable planar shell in three-dimensional space. The Free Mesh Technique [34] is employed to create the mesh. To find the largest practical element size for acceptable numerical accuracy with minimum computing time the authors first conducted a convergence study. As a representative example, the plate with the $[90/\pm45/0_9]_s$ lay-up was chosen, with the plate having square elements of varying side dimensions in the range of 10 to 90 mm at 10 mm increments. The failure stress (σ_{fail}), from a *second-order buckling analysis* and the ultimate compressive stress (σ_c), from a *first-order compressive analysis* (both to be introduced later), were obtained and plots were constructed with element side dimension. Because it was found that a side dimension of ca. 40 mm (41.6 mm or 12 elements along a 500 mm length) or lower results in converged results (i.e., variation less than 5%), this element size was adopted to construct the finite element models.

The simply supported displacement boundary condition was modelled by constraining to zero out-of-plane displacements (i.e., perpendicular to the plane surface) along all four sides of the plates. Moreover, modelling required restraining the (mid-surface) in-plane displacement perpendicular to the loaded 0-direction along the side and opposite to the compressed (loaded) side, and the in-plane displacement parallel to the load direction along the non-loaded sides. Next, the rotation along the four sides was permitted to simulate the condition of knife edge supports for the simply supported boundary condition.

Compression load was modelled by applying a constant axial displacement along the side without in-plane displacements set to zero. Using the variables presented in Tables 1–4 a total of 156 different plate models were solved using ABAQUS®. 78 of these plates are of E-glass-epoxy and the other 78 plates are of carbon-epoxy. Each material group of 78 plates consists of 18 plates of UD, 0-dominated or Quasi-isotropic lay-ups and 24 plates of 45-dominated lay-ups. To manage this large number of analyses a Python script was written to create and solve the simulations, and to export the output results for processing and evaluation.

2.3. Numerical analysis

The elastic critical loads and shapes of the first buckling mode are obtained from linear Eigenvalue analyses (first-order modelling). It is the shape of the first buckling mode that is employed to introduce into the mesh specification the initial geometrical imperfection, as specified in Table 4. Modelling of the geometrical imperfection is by having double curvature over the square mesh of 500 × 500 mm with the maximum out-plane-displacement at the centre.

In post-buckling analysis the effects of large deformations (> half the plate's thickness) are considered to make the modelling a non-linear geometrical analysis. Riks analysis is used in ABAQUS® to extract the non-linear post-buckling behaviour. Hashin failure criteria [35] are adopted for an integrated progressive failure analysis. Including progressive failure in the non-linear Riks analysis approach does create possible numerical convergence difficulties owing to severe softening behaviour and element stiffness degradation. To overcome this computational problem, the modelling methodology introduces viscous regularization, as offered as an analysis option in ABAQUS® [36]. To

prevent any troublesome numerical divergence, this scheme regulates the tangent stiffness matrix of elements to be positive for small time increments and stabilizes the damage evolution problem by introducing viscosity coefficients into the material modelling [34]. The progressive failure and the adoption of material stiffness degradation in the modelling are explained in Section 2.4.

Three types of structural analyses are conducted to calculate the necessary parameters required to construct buckling curves, and they are:

(i) *Linear elastic buckling analysis*: to obtain the relevant eigenmodes and eigenvalues to the first buckling mode and the elastic critical buckling stress, σ_{crit}. In this analysis a compressive load, P, of 1000 kN is applied as a shell edge load along the loaded side to perform this type of analysis. The elastic critical buckling stress was calculated by:

$$\sigma_{crit} = \frac{(Eigenvalue) \times P}{A} \tag{1}$$

where A is the plate's cross-sectional area, given by 500 times the plate's thickness (see Table 3).

(ii) *Second-order post-buckling analysis*: to predict the failure stress, σ_{fail}, defined as the maximum load along the ABAQUS®-generated load–displacement curve divided by the plate's cross-sectional area (A). σ_{fail} is required to determine the buckling reduction factor, χ, as introduced in Section 3. This non-linear buckling analysis allows for non-linear deformations to be determined for the compressed plates with their predefined initial geometrical imperfections (see Table 4). To apply the compression load in the second-order buckling analyses, all the nodes along the loaded side of the plates are constrained to a master node to which the predefined displacement is introduced. To capture the behaviour after instability the Riks analysis is employed with ABAQUS® using the arc-length on the static equilibrium path in the load–displacement space. The arc-length is not constant with the user controlling the size of the steps and normally when the numerical solution tends to be unstable the step size is adjusted, and the iterative solution is calculated back and forth around the point of instability until it gets through. The value of the pre-defined displacement ranges from 5.5 to 13 mm, being dependent on the lay-up as defined in Table 2.

(iii) *First-order linear analysis*: to calculate the ultimate compressive strength, σ_c, of the laminates. This strength is defined as the maximum stress from the ABAQUS®-generated compression load–deformation curve and is required to determine both the buckling reduction factor, χ, and slenderness $\bar{\lambda}$ (see Section 3). Numerical analysis is performed in the same way as the second-order post-buckling analysis of (ii), but now without the modelling including initial imperfections and second-order effects. Importantly, these first-order simulations do involve linear elastic behaviour before damage initiation and progressive degradation of element stiffness using the Hashin ply-level failure criteria following initiation of failure in the first ply.

2.4. Progressive failure

The concept of progressive failure employed in the analysis is based on successively reducing a plate's stiffness by reducing certain ply-level element stiffnesses as plies undergo progressive damage. Different failure criteria are used to capture the initiation and propagation of the damage, and ABAQUS® offers the modelling option to simulate anisotropic damage in FRP laminates. Because the response of undamaged FRP material is linearly elastic, the modelling methodology can neglect any plastic deformations since they are not necessary for the analysis of FRP laminates. As mentioned earlier, Hashin's failure criteria [35] are employed at the ply-level in the elements to predict the onset of damage, and the damage evolution law for progressive failure is based on energy dissipation during the damage process and the assumption applied in ABAQUS® modelling for linear material softening [34]. In other words, the stress–strain curve after the damage initiation (maximum stress) reduces linearly to zero at the maximum strain value. Input values of fracture energies for the damage evolution laws were established by the authors by back-calculation after using ABAQUS® to numerically simulate the test results reported in [33]. More detailed information about these simulations can be found in [37]. The damage analysis used in this study has material stiffness degradation at the ply level in elements, and the stress–strain response of the laminate is defined by [34]:

$$\sigma_c = C_d \cdot \varepsilon_c \tag{2}$$

where:

σ_c is the compressive direct stress,

ε_c is the compressive direct strain,

C_d is the elasticity matrix that reflects damage within a ply, and is expressed by:

$$C_d = \frac{1}{D} \times \begin{bmatrix} (1-d_f)E_{11} & (1-d_f)(1-d_m)\nu_{12}E_{11} & 0 \\ (1-d_f)(1-d_m)\nu_{12}E_{22} & (1-d_m)E_{22} & 0 \\ 0 & 0 & (1-d_s)G_{12} \times D \end{bmatrix} \tag{3}$$

where:

$D = 1-(1-d_f)(1-d_m)\nu_{12}\nu_{21}$,

d_f is the current state of the fibre damage,

d_m is the current state of the matrix damage,

d_s is the current state of the shear damage,

E_{11} is the modulus of elasticity in the fibre direction (Table 1),

E_{22} is the modulus of elasticity in the direction perpendicular to fibre direction (Table 1),

G_{12} is the in-plane shear modulus (Table 1),

ν_{12} and ν_{21} are Major and Minor Poisson's ratios (Table 1), with $\nu_{21} = \nu_{21}.(E_{22}/E_{11})$.

Note that the elastic constants for plies of both the E-glass-epoxy and carbon-epoxy FRP materials are reported in Table 1.

Damage initiation refers to the onset of material degradation at a point within a ply. In ABAQUS® the failure criteria for damage initiation can be based on Hashin's theory [35], which considers the four different damage initiation mechanisms of: fibre tension failure; fibre compression failure; matrix tension failure; and matrix compression failure. The formulae being continually checked (at ply-level and in every element) for the status of these criteria are:

$$\text{Fibre tension } (\hat{\sigma}_{11} \geq 0): F_f^t = \left(\frac{\hat{\sigma}_{11}}{X^T}\right)^2 + \alpha\left(\frac{\hat{\tau}_{12}}{S^L}\right)^2 \tag{4}$$

$$\text{Fibre compression } (\hat{\sigma}_{11} < 0): F_f^c = \left(\frac{\hat{\sigma}_{11}}{X^C}\right)^2 \tag{5}$$

$$\text{Matrix tension } (\hat{\sigma}_{22} \geq 0): F_f^t = \left(\frac{\hat{\sigma}_{22}}{Y^T}\right)^2 + \left(\frac{\hat{\tau}_{12}}{S^L}\right)^2 \tag{6}$$

$$\text{Matrix compression } (\hat{\sigma}_{22} < 0): F_m^c = \left(\frac{\hat{\sigma}_{22}}{2S^T}\right)^2 + \left[\left(\frac{Y^C}{2S^T}\right)^2 - 1\right]\frac{\hat{\sigma}_{22}}{Y^C} + \left(\frac{\hat{\tau}_{12}}{S^L}\right)^2 \tag{7}$$

The variables in Eqs. (4) to (7) are:

F is the failure index for a failure criterion that when < 1.0 there is no failure and when equal to 1.0 or higher there is failure,

t and c are superscripts with the failure index for tension and compression,

f and m are subscripts with the failure index for fibres and matrix,

X^T is the longitudinal tensile strength (value in Table 1),

X^C is the longitudinal compressive strength (value in Table 1),
Y^T is the transverse tensile strength (value in Table 1),
Y^C is the transverse compressive strength (value in Table 1),
S^L and S^T are the longitudinal and transverse shear strengths that take the value of S^{LT} in Table 1.

The original form of Eq. (4) has coefficient α that determines the contribution of the shear stress to the fibre tensile damage initiation criterion. By setting α to 0 and $S^T = 0.5Y^C$ the failure criterion is set to the form proposed by Hashin and Rotem [38], while setting α to 1.0 yields the form by Hashin [35] that has been adopted in this study.

$\hat{\sigma}_{11}, \hat{\sigma}_{22}, \hat{\tau}_{12}$ are the components of the effective stress tensor $\hat{\sigma}$ at the ply level in an element used to evaluate the initiation criteria, which is computed by:

$$\hat{\sigma} = \mathbf{M}\sigma \tag{8}$$

where vector σ is the true stress and $\mathbf{M}$ is the damage operator and expressed according to:

$$\mathbf{M} = \begin{vmatrix} \frac{1}{(1-d_f)} & 0 & 0 \\ 0 & \frac{1}{(1-d_m)} & 0 \\ 0 & 0 & \frac{1}{(1-d_s)} \end{vmatrix} \tag{9}$$

In Eq. (9) d_f, d_m and d_s are internal (damage) variables that characterize fibre, matrix and shear damage within a ply within an element, and derived from the damage variables d_f^t, d_f^c, d_m^t and d_m^c, which correspond to the four mechanisms as follows:

$$d_f = \begin{Bmatrix} d_f^t \text{ if } \hat{\sigma}_{11} \geq 0 \\ d_f^c \text{ if } \hat{\sigma}_{11} < 0 \end{Bmatrix} \tag{10}$$

$$d_m = \begin{Bmatrix} d_m^t \text{ if } \hat{\sigma}_{22} \geq 0 \\ d_m^c \text{ if } \hat{\sigma}_{22} < 0 \end{Bmatrix} \tag{11}$$

$$d_s = 1 - \left(1 - d_f^t\right)\left(1 - d_f^c\right)\left(1 - d_m^t\right)\left(1 - d_m^c\right) \tag{12}$$

Because none of 156 plates analysed are loaded with a shear component it has been appropriate in the modelling methodology to ignore any in-plane shear-generated failure. Prior to any damage initiation and evolution, the damage operator, $\mathbf{M}$, in Eq. (9) is equal to the identity matrix, so that $\hat{\sigma} = \sigma$. Once damage initiation and damage progression exist for at least one of the four failure mechanisms defined by Eqs. (4) to (7), $\mathbf{M}$ becomes significant in the criteria for damage initiation of the other mechanisms. Based on effective stress levels calculated during ABAQUS® analyses from Eq. (9) the three damage variables by Eqs. (10) to (12) are determined at each integration point in every element in all plies, and they take different values for fibre and matrix and for tension and compression stresses. The ABAQUS® analysis uses Eqs. (4) to (12) to reduce the plate's stiffness in the non-linear analysis (ii) (refer to Section 2.3) by way of progressive reductions in elements and plies as the compression loading increases above its value for the initiation of first ply failure (which occurs first in one element and one ply and shall be one of the four failure mechanisms).

3. Generation of buckling curves

The hypothesis for this study is that it is practical to create non-dimensional buckling curves for failed FRP plates with different lay-ups that has a consistent format to the flexural buckling curves (for design of column members of steel) in Eurocode standard EN 1993-1-1:2005 (6.3.1.2). For steel, the abscissa axis for the slenderness, $\bar{\lambda}$, and ordinate axis for the buckling reduction factor χ, are defined by:

$$\bar{\lambda} = \sqrt{\frac{f_y}{\sigma_{cr}}} \tag{13}$$

$$\chi = \frac{\sigma_{max}}{f_y} \leq 1.0 \tag{14}$$

where:
f_y is the yield strength of the grade of steel,
σ_{cr} is the elastic critical stress for the relevant buckling mode based on the gross cross-sectional properties of the section,
σ_{max} is the maximum stress at ultimate failure.

To create equivalent buckling curves for simply-supported FRP plates (subjected to uniform uniaxial and in-plane compression), we replaced f_y with σ_c (predicted by ABAQUS® first-order compression analyses (iii)) and σ_{max} with σ_{fail} (predicted by ABAQUS® second-order buckling analyses (ii)). This transforms Equations (13) and (14) to be:

$$\bar{\lambda} = \sqrt{\frac{\sigma_c}{\sigma_{crit}}} \tag{15}$$

$$\chi = \frac{\sigma_{fail}}{\sigma_c} \tag{16}$$

where:
σ_c is the compressive strength (or crushing strength) of the plate (without geometrical imperfection) using ABAQUS® first-order analysis (iii),
σ_{crit} is the elastic critical buckling stress obtained from Eq. (1),
σ_{fail} is the ultimate compressive stress for plate failure, considering the post-buckling behaviour, obtained from non-linear Riks analysis (with geometrical imperfection).

4. Results and discussion

4.1. Second-order post-buckling analysis

Plotted in Figs. 1(a) to 1(d) are curves for compression load, P, with out-of-plane deformation (at centre of the square plates) for laminates having different FRP materials, ply lay-ups, thicknesses and initial geometrical imperfection, as specified in Tables 1–4. In the four plots the black curves (lowest group of three), dark grey (middle group) and light grey (top group) coloured curves are for thicknesses of 9.6 (number 2), 19.2 (number 4) and 24 mm (number 5), respectively. As can be seen from the curves in the figures, increasing the initial imperfection from $b/10{,}000$ to $b/100$ ($b = 500$ mm) results numerically in a diminishing bifurcation-response for a smoother transition into the post-buckling region (i.e., continuous deformation under increasing P, without sudden deformations associated with drastic changes in structural plate stiffness). It can be seen from the characteristics of the curves that the initial imperfection magnitude also has different effects on the ultimate load, which gives us σ_{fail}. For plates analysed with relatively high slenderness (i.e., $x = 2$ for smallest thicknesses (refer to Table 2)) the magnitude of the initial imperfections did not adversely affect the ultimate compression load. However, for plates analysed with relatively medium and low slenderness (when $x = 4$ and 5), in which their critical stresses for elastic buckling are close to the compressive strength of the laminates, there is higher sensitivities to imperfection magnitudes and reductions in ultimate load carrying capacities become significant, as seen in Figs. 1(a) to 1(d). Such a response of imperfect plates subjected to compression is observed also when the material is steel (before yielding), and this fact justifies why the strength capacity is governed by the internal compressive stress redistribution after buckling. These findings agree with experimental test results on FRP plates reported by Fallah *et al.* [20] and Hayman *et al.* [33]. Based on the known physical behaviour we have that σ_{fail} is determined on dividing the maximum P by the cross-sectional area of the plate, A.

4.2. Compressive strength

Determined using first-order compressive analyses Figs. 2(a) to 2(d) present a series of load (P) with in-plane displacement curves for several different plates whose labels are defined by content in Tables 1–5. Note that constant variables are for the FRP material being

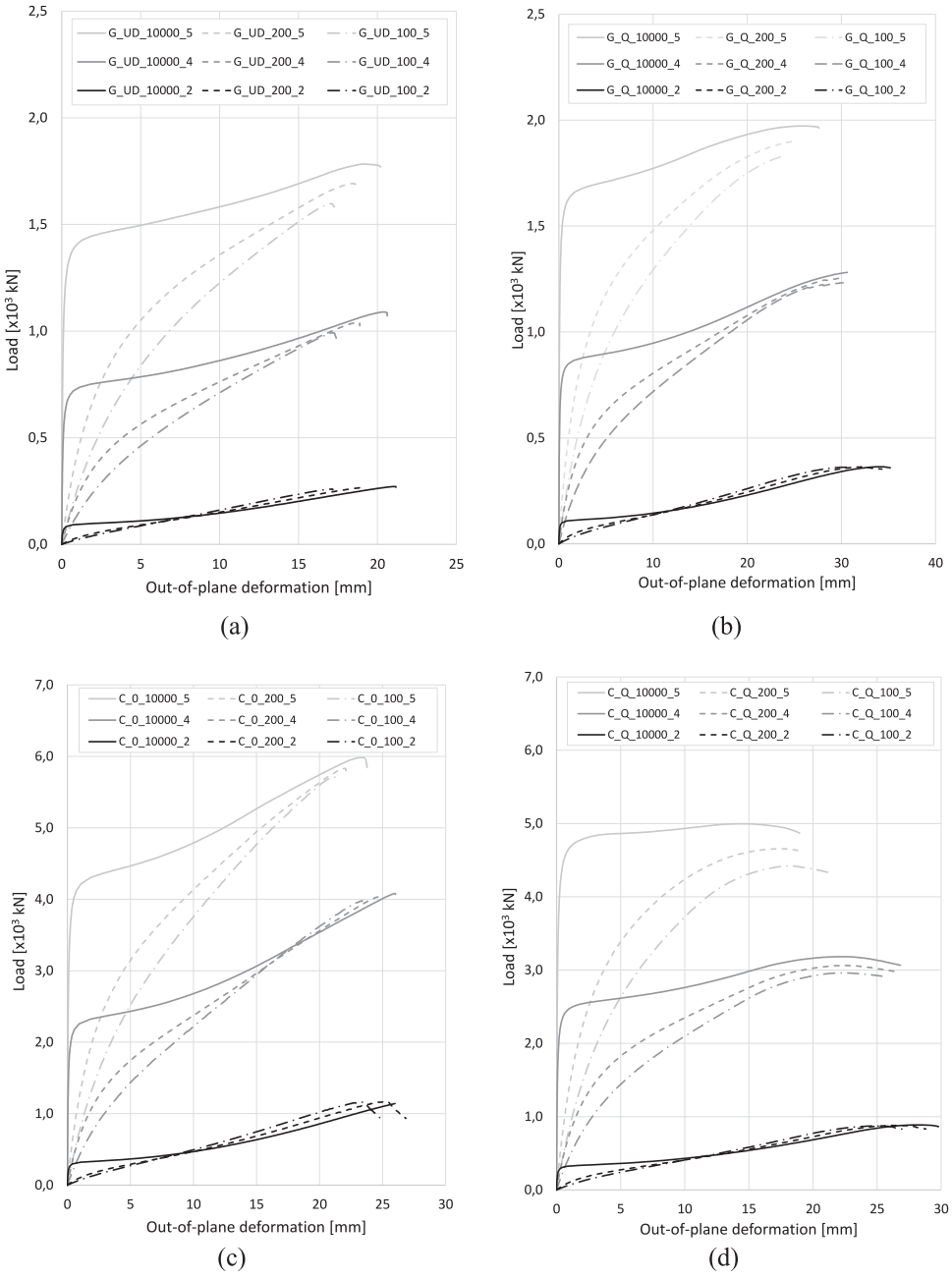

Fig. 1. Compression load with out-of-plane displacement curves for different plates defined from Tables 1–5: (a) plate G_UD_Z_T; (b) plate G_Q_Z_T; (c) plate C_0_Z_T; (d) plate C_Q_Z_T. (Z = 10,000; 200; 100 (correspond to 0.05, 2.5 and 5 mm imperfection), and $T = 2$, 4, 5 corresponding plate thicknesses of 9.6, 19.2 and 24 mm.)

E-glass-epoxy and the initial geometrical imperfection being 0.05 mm (b/10,000). Figs. 2(a) and 2(b) are for the UD and 0-dominated lay-up plates, and as expected the characteristics of the six curves for the changing thicknesses (in both parts of the figure) show a structural response that is linear elastic up to sudden (ultimate) failure (for σ_c) indicated by a knee and a dramatic reversal in plate flexural stiffness. As can be seen in Figs. 2(c) and 2(d), the response of both 45-dominated and quasi-isotropic lay-ups is for a progressive failure, with the onset of buckling signalled by a lowering of plate flexural stiffness, and then at a higher compression stress, there is an ultimate failure (for σ_c), as indicated by a reversal in plate stiffness. For several thicknesses there is a second reduction in stiffness owing to first ply failure (but not more ply failures) before the ultimate compression load is reached. Extracted from the curves is the compressive strength, σ_c, which is calculated by dividing the maximum P in the plots by the cross-sectional area of the plate, A, which is 500 times the thickness (see Table 3).

4.3. Results of the parametric study

Plotted in Fig. 3 is the buckling reduction factor χ (given by Eq. (15)) with (relative) slenderness $\bar{\lambda}$ (given by Eq. (16)) using the results from analyses of 156 plate variations of FRP materials, lay-ups, thicknesses and initial geometrical imperfections (as defined using data in Tables 1–4). Numerical results are for square plates 500 × 500 mm having simply supported boundary conditions and subjected to uniform uniaxial and in-plane compression. In Fig. 3 are plotted 24 buckling curves. For each of the four lay-ups (Table 2), the two fibre types (Table 1) we have set of three curves, which are for the three imperfections (Table 4) and slenderness values are given by the eight thicknesses

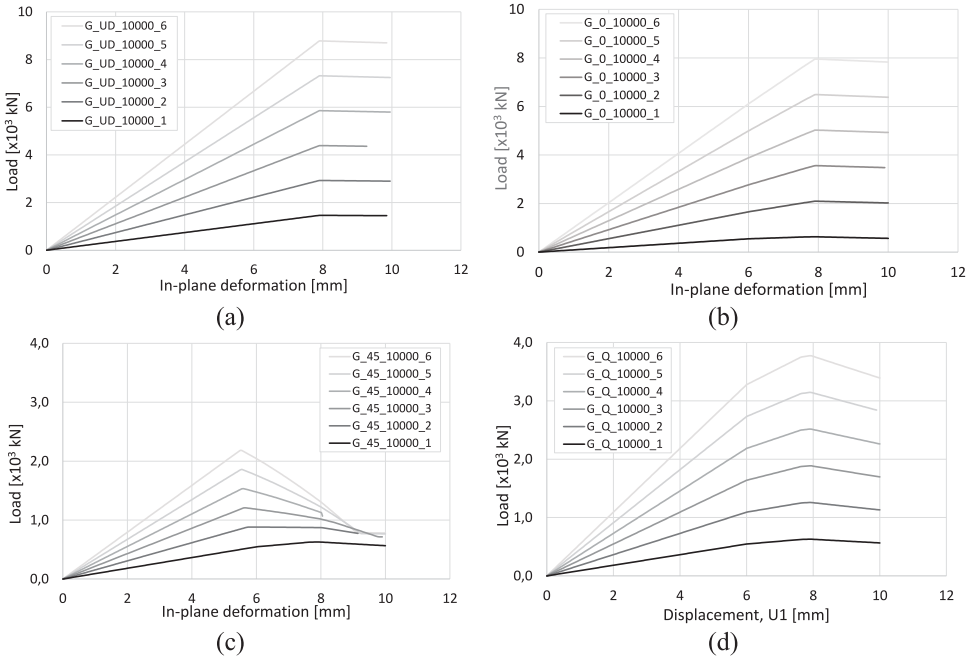

Fig. 2. Curves for compression load with in-plane deformation from first-order failure analyses for different thicknesses of plates: (a) G_UD_10,000_T; (b) G_0_10,000_T; (c) G_45_10,000_T; (d) G_Q_10,000_T.

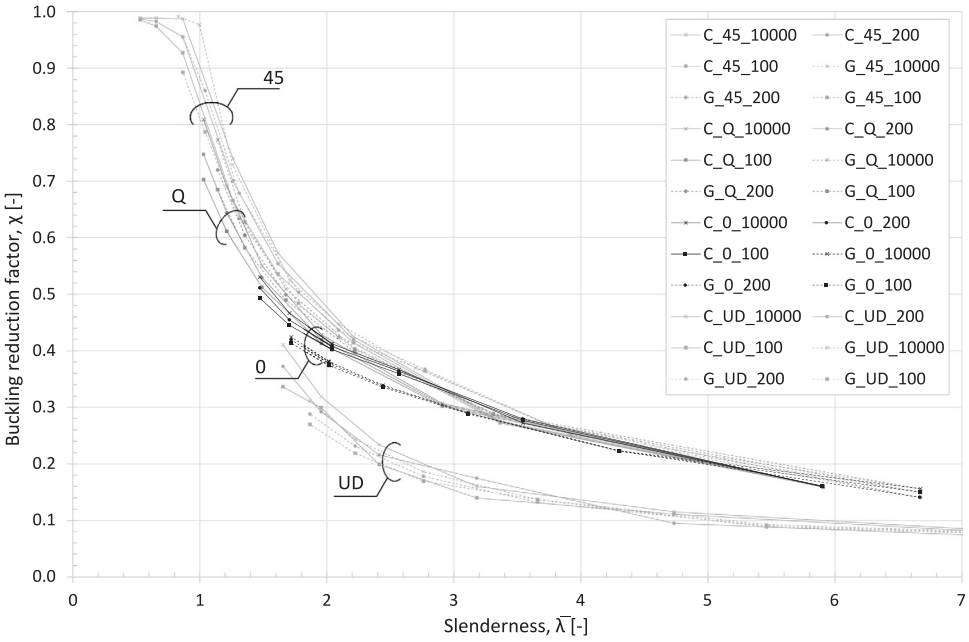

Fig. 3. Buckling reduction factor χ plotted with slenderness $\bar{\lambda}$ for all 156 laminated plates.

(Table 3) with the 45-dominate lay-ups and six thicknesses (Table 3) for the other three lay-ups (Table 2). It can be observed that these 24 buckling curves follow two distinct trends specified by grouping together the six UD plate curves or the 18 multi-directional plate curves. The order in which Table 2 lay-up curves appear in the plotting (from top to bottom) is: 45-dominated; quasi-isotropic; 0-dominated; UD. Regarding the difference in the $\chi - \bar{\lambda}$ relationships between the UD group and multi-directional group, it is observed that the UD-generated curves are considerably below the rest of the curves, with the highest χ at about 0.4. χ is observed to approach 1.0 from the analyses of the 120 plates within the other group. This finding is attributed to how UD plates fail. Prior to the initiation of buckling deformations, the compressive stress is uniformly distributed within these plates. When buckling failure occurs UD plates lose stiffness in the 'buckled' region and there is an internal stress redistribution to the 'stiffer' areas around the simply supported sides, where there are no or small 'buckling' deformations. Fig. 4(a) illustrates the uniform compression stress states throughout a UD plate prior to buckling. As depicted in Fig. 4(b) the post-buckling mechanism is associated with the formation of a transverse tension band as illustrated by the stress field arrows in the figure. Because the Transverse tensile strength of UD laminates (from Table 1, Y^T for the E-glass-epoxy material is 31 MPa and for carbon-epoxy Y^T is 43 MPa) is a matrix governed strength, there is little, if no post-buckling reserve strength compared to laminates of the other

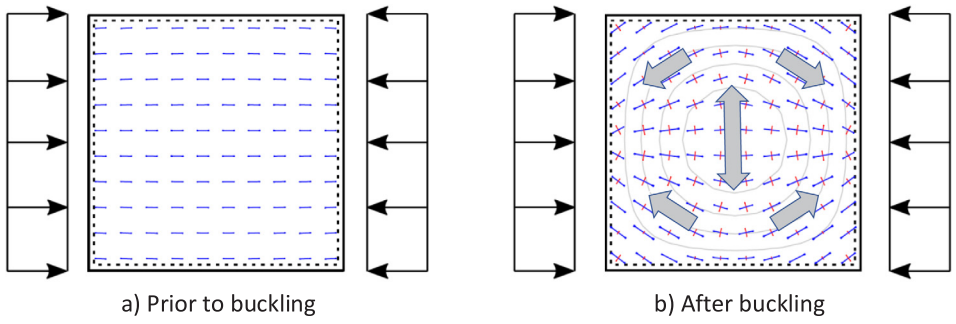

Fig. 4. (a) Plate subjected to compression loads before buckling: (b) Plate after buckling and the formation of the transverse tension band.

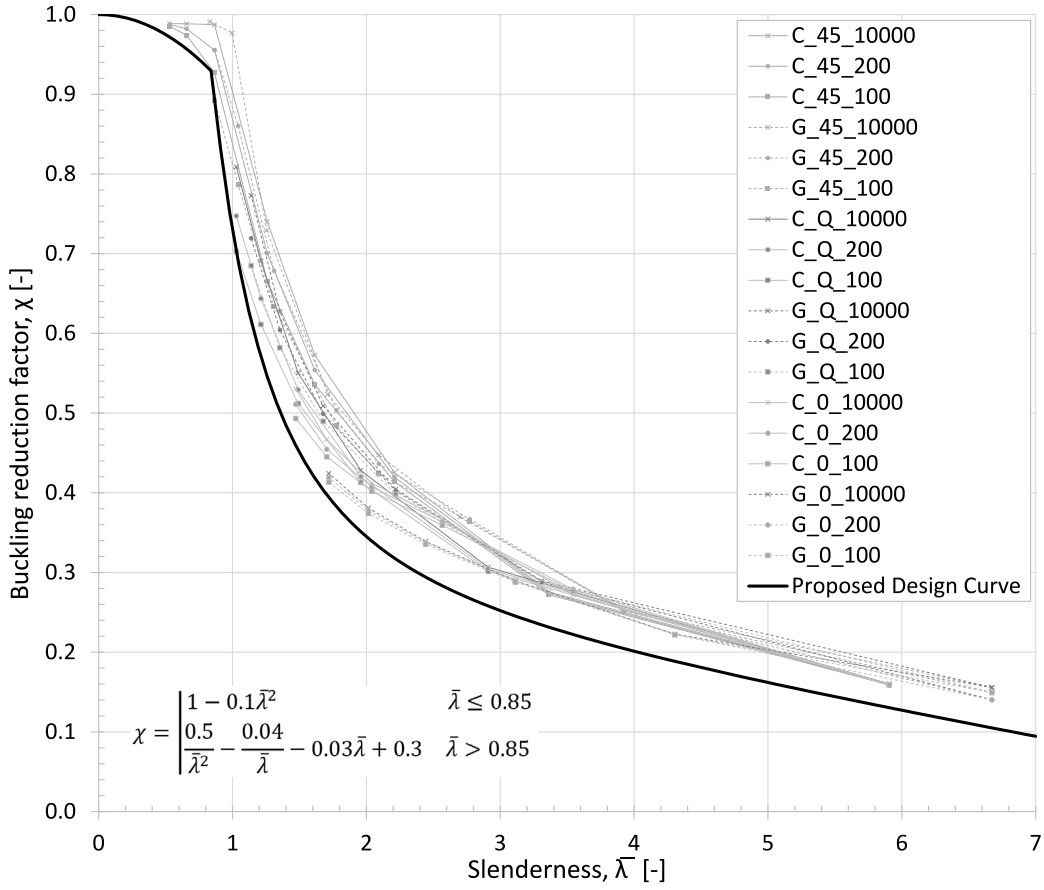

Fig. 5. Buckling reduction factor χ with slenderness $\bar{\lambda}$ for quasi-isotropic, 0- and 45-dominated lay-ups and a fitted curve (coloured black) to the lower-bound defined by Equations (17) and (18).

lay-ups that possess higher transverse strengths because a proportion of fibres are reinforcing in that direction. Moreover, the microstructure of UD laminates in the transverse direction (combination of stiffer fibres and softer matrix) results in stress concentrations negatively affecting the transverse strength. It is noted that because UD laminates have this structural weakness, they are not found in FRP structures where these thin-walled elements are subjected to compressive forces. This technical fact is justification not to include UD laminates in Section 5 where the authors present a proposed design buckling curve that scopes multi-directional lay-ups.

5. Design buckling curve

Based on using the numerical results from all multi-directional lay-ups, the plotting in Fig. 5 introduces a non-dimensional design buckling curve (the thick black solid curve) defined as the lower bound of all the $\chi - \bar{\lambda}$ curves. The authors constructed the shape of the curve by visual inspection using Maple® software with quadratic functions of slenderness $\bar{\lambda}$. Fig. 5 is also Fig. 3 without the six UD buckling curves. The formulae to the proposed curve can be expressed as:

$$\chi = 1 - 0.1\bar{\lambda}^2 \qquad \bar{\lambda} \le 0.85 \qquad (17)$$

$$\chi = \frac{0.5}{\bar{\lambda}^2} - \frac{0.04}{\bar{\lambda}} - 0.03\bar{\lambda} + 0.3 \qquad \bar{\lambda} > 0.85 \qquad (18)$$

For a preliminary validation, the proposed ABAQUS®-generated buckling design curve in Fig. 5 is benchmarked using experimental data taken from the literature. For this preliminary validation process the authors used test results taken from Refs. [33,39–41]. Table 6 lists data on the glass and carbon fibre laminates in these four studies. The relatively small number of benchmark points is attributed to the

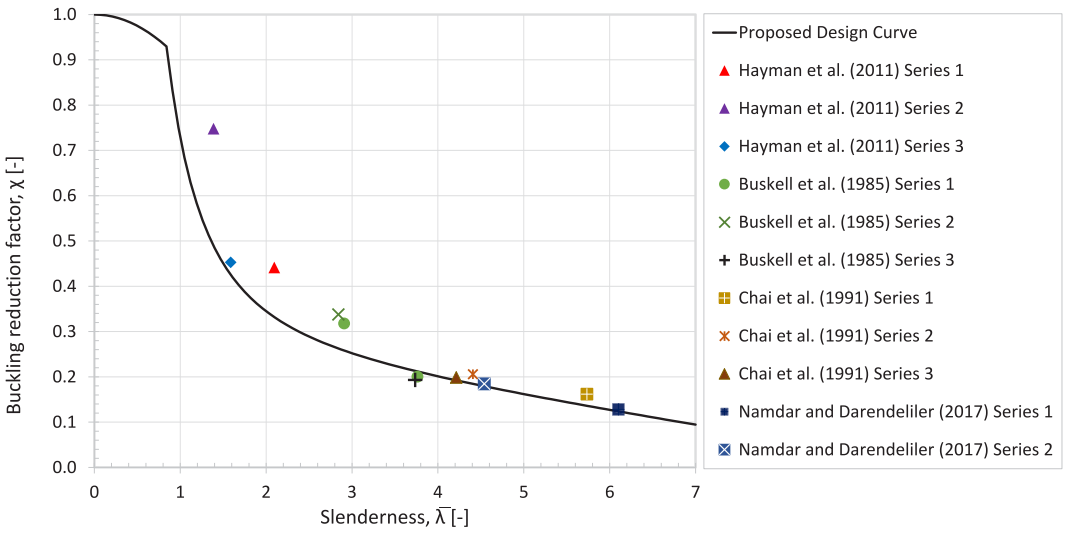

Fig. 6. Proposed design buckling curve given by buckling reduction factor χ with slenderness $\bar{\lambda}$ that is benchmarked against experimental test results in the literature.

limited number of previous studies sourced by the authors with post-buckling behaviour of unstiffened 'simply supported' plates subjected to uniform uniaxial and in-plane compression that provides the necessary information to calculate the non-dimensional parameters $\bar{\lambda}$ and χ. The authors sought to find the closest experimental match to the numerically simulated FRP plates to maintain a reliable benchmarking. Table 6 presents the relevant data for experiments used in the benchmarking process. It should be noted that not all the tested plates are square, and the authors are aware that on buckling complete half-sine waves might not have formed. Theory informs us that such plates will, theoretically, buckle at higher loads and so the presented ABAQUS®-generated buckling curve in Eqs. (17) and (18) should provide safe predictions to elastic critical buckling loads. What is not known is the behaviour of such plates in the post-buckling regime and the influence of the goverening initial geometrical imperfection on their strengths. Although the authors believe that ABAQUS®'s modelling and simulation are reliable in accounting for these effects further research work is needed to confirm our understanding. For the sake of completeness, the authors have included test results for rectangular plates with and without integer side-length aspect ratios. In Fig. 6 the experimental data points are plotted with the design buckling curve (thick black solid line). Non-dimensional parameters χ and $\bar{\lambda}$ for the test results were back calculated using the reported plate properties and ultimate failure loads tabulated in Table 6.

Table 6 has 13 columns, with column (1) listing the references to a total of 45 test results, which are distributed into 11 test series. Column (2) gives the balanced symmetrical lay-ups for the multi-layered FRP plates that always have 0° and 45° fibre orientations. Six of the 11 laminations also have fibre reinforcement oriented at 90°. In column (3) are listed the number of test results in a series, which range from one to eight. Column (4) is for the FRP plies being either of Glass-Epoxy (GE) or Carbon-Epoxy (CE). Laminate thicknesses are reported in column (5), and t is from 1.75 to 20 mm. It is noted that only the plates in the three experimental series with Hayman *et al.* [33] had a thickness in the range scoped in the ABAQUS® simulations; all others are <4.8 mm, which is the minimum thickness in Table 3. Column (6) is for the width of the plate (b) subjected to the uniform uniaxial compression, and column (7) is for the plate aspect ratio (l/b), with l the length of the plate. The aspect ratios are in range of 1.0 to 5.09, with, again, only the series from Hayman *et al.* satisfying the ABAQUS® ratio of 1.0. Columns (8) to (10) report mean results for the three stress values of σ_c, σ_{crit} and σ_{fail} in Eqs. (15) and (16) required to calculate the non-dimensional parameters $\bar{\lambda}$ and χ, which are presented in columns (12) and (13). Finally, column (11) in Table 6 is for the strength ratio $\sigma_{fail}/\sigma_{crit}$ that gives, for the series of plates, a numerical value for the failure load in terms of critical elastic buckling load. It is observed that this ratio ranges from 1.1 to 5.3.

As seen from column (12) in Table 6 the test results effectively cover a descent range of slenderness ratios, $\bar{\lambda}$, from 1.4 to 6.1. Plotted in Fig. 6 are the mean buckling reduction factor χ for the 11 series of tests (can be with a single plate). Hayman *et al.* [33] provides to the benchmarking exercise 20 test results. They comprise: seven points from Series 1 (red triangle symbol); six from Series 2 (purple triangle symbol); and seven from Series 3 (blue diamond). Another three contributions provide a total of 25 test results. Researchers Buskell *et al.* [39] provide four points comprising Series 1 of two single tests (two green circle symbols) and Series 2 (dark green cross symbol) and 3 (deep purple plus symbol) for a single test result each. The experimental program conducted by Chai *et al.* [37,40] provides 19 points, comprising Series 1 of eight test results (white cross inside a tawny square symbol), Series 2 with seven data points (red cross and red vertical line symbol), and Series 3 for four tests (brown triangle symbol). Finally, the experimental work of Namdar and Darendeliler [38,41] provides two data points from Series 1 (dark blue square) and 2 (white cross in blue square) with a single test result each.

Overall, it is seen from the plotted mean test results that the proposed design curve (thick black line in Fig. 6), given by Eqs. (17) and (18), establishes, and on the low side, the experimental evidence for post-buckling strengths with reasonable agreement, particularly for $\bar{\lambda} > 1.5$. This is a promising outcome given the complexities in conducting buckling experiments that reliably corresponded to the input data in ABAQUS® simulations. The observed deviations, of course, are attributed not only to the research methodology used to generate the proposed curve, but also to several experimental sources of uncertainties, such as from: plate aspect ratio, variability in ply material properties; geometrical and other imperfections; effect of real boundary conditions and loading rate effect.

Plotted in Fig. 7 are 120 ABAQUS®-generated ratios for $\sigma_{fail}/\sigma_{crit}$ with plate slenderness, $\bar{\lambda}$. The magnitude of the ratio gives the increased strength gain on taking the ultimate failure load rather than the critical elastic buckling load, as is recommended in CEN/TS 19101:2022 [13]. The information in Fig. 7 for multi-directional plates offers a useful design aid in the sense that it can be used for a prediction of σ_{fail}, providing the user has knowledge of σ_{crit} and $\bar{\lambda}$. To obtain reliable and

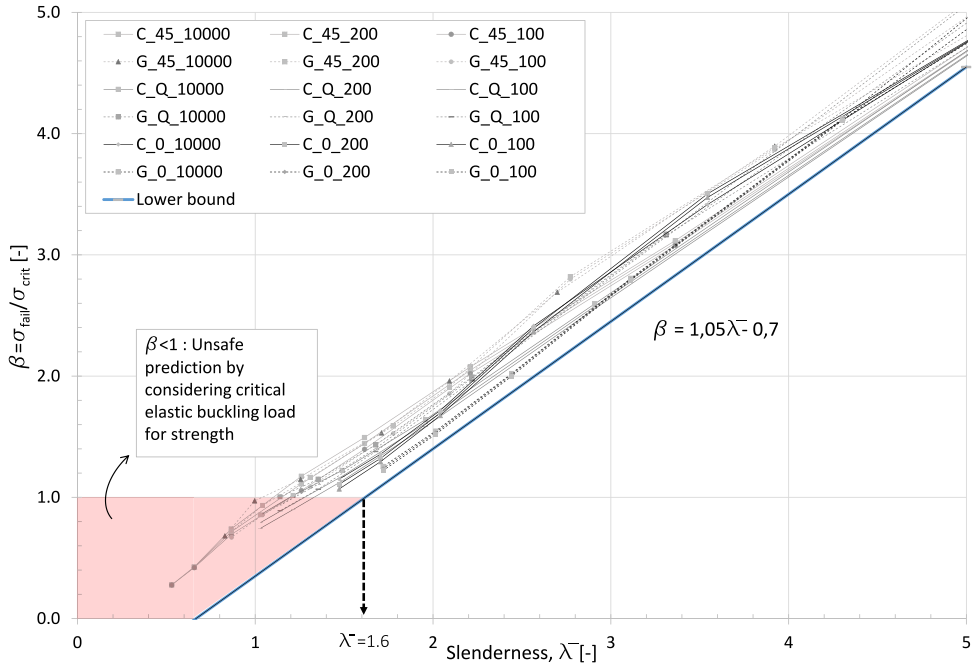

Fig. 7. $\sigma_{fail}/\sigma_{crit}$ with slenderness for the 156 plates in the ABAQUS® study.

Table 6
Properties of FRP plates used to benchmark the proposed design buckling curve.

Reference	Lay-up	No of tests	Mat.	t [mm]	Plate size (b) [mm]	l/b[c]	σ_c [MPa]	σ_{crit} [MPa]	σ_{fail} [MPa]	$\sigma_{fail}/\sigma_{crit}$	$\bar{\lambda}$	χ
(1)	(2)	(3)	(4)	(5)	(6)	(7)	(8)	(9)	(10)	(11)	(12)	(13)
Hayman *et al.* (2011) Series 1 [30]	$[\pm 45/0_4/\pm 45/0_3]_S$	7	GE[a]	9.7	320	1.0	233	53	103	1.8	2.10	0.44
Hayman *et al.* (2011) Series 2 [30]	$[\pm 45/0_4/\pm 45/0_4/\pm 45/0_3]_S$	6	GE	15	320	1.0	234	121	175	1.4	1.39	0.75
Hayman *et al.* (2011) Series 3 [30]	$[\pm 45/0_4/\pm 45/0_4/\pm 45/0_2]_S$	7	GE	20	320	1.0	747	296	338	1.1	1.59	0.45
Buskell *et al.* (1985) Series 1 [39]	$[0/90/45/-45]_{2S}$	1	CE[b]	2	113	3.04	837	59.1	168	2.8	3.76	0.20
		1		2	94	3.56	837	98.9	266	2.7	2.91	0.32
Buskell *et al.* (1985) Series 2 [39]	$[0/45/-45/90]_{2S}$	1	CE	2	94	3.56	838	104	283	2.7	2.84	0.34
Buskell *et al.* (1985) Series 3 [39]	$[45/0/-45/90]_{S2}$	1	CE	2	113	3.04	837	60.0	162	2.7	3.74	0.19
Chai *et al.* (1991) Series 1 [40]	$[45/0/0/90/0/-45/0]_S$	8	CE	1.75	120	3.82	1107	33.7	179	5.3	5.74	0.16
Chai *et al.* (1991) Series 2 [40]	$[45/0/0/90/0/-45/0]_S$	7	CE	1.75	90	5.09	1107	57	228	4.0	4.41	0.21
Chai *et al.* (1991) Series 3 [40]	$[45/0/0/90/0/-45/0]_S$	4	CE	1.83	90	5.09	1107	62.4	220	3.5	4.21	0.20
Namdar and Darendeliler (2017) Series 1 [41]	$[45/0/45/0/45]_S$	1	CE	2.80	330	1.21	657	17.6	84.2	4.8	6.10	0.13
Namdar and Darendeliler (2017) Series 2 [41]	$[45/-45/0/45/90/90/-45/0]_S$	1	CE	2.94	330	1.21	471	22.9	86.9	3.8	4.54	0.18

[a]Glass fibre-epoxy.
[b]Carbon fibre-epoxy.
[c]Aspect ratio (length/width).

conservative predictions for σ_{fail} a lower-bound curve has been introduced in Fig. 7, and the blue coloured curve has the linear trendline formula:

$$\beta = \frac{\sigma_{fail}}{\sigma_{crit}} = 1.05\bar{\lambda} - 0.7 \tag{19}$$

It is to be noted that when plates are 'stocky' with relatively low slenderness the mode of failure can be by material strength (i.e., σ_{fail} is σ_c). Now we have $\sigma_{fail}/\sigma_{crit} < 1$ and Eq. (19) is invalid. In Fig. 7 the salmon pink shaded area in the bottom left is the zone where using the critical elastic buckling load in design can result in misleading strength predictions. Based on the lower-bound approximation given by Eq. (19) the value of $\bar{\lambda}$ below which this phenomenon exists is 1.6. It is concluded that it is necessary to pay more attention to the mode of failure when designing FRP plates that have a 'stocky' slenderness. Regarding the test results presented in Table 6 only Series 2 and 3 by Hayman *et al.* [33] is with $\bar{\lambda} < 1.6$. As seen from Table 6 the values of $\sigma_{fail}/\sigma_{crit}$ for these two series are significantly smaller than the rest of the series.

6. Concluding remarks and future work

The aim of this numerical study has been to investigate the feasibility of proposing a unified non-dimensional design buckling curve (buckling reduction factor with slenderness) for laminated plates of Fibre Reinforced Polymer (FRP) materials subjected to uniform uniaxial and in-plane compression. A parametric study using ABAQUS® modelling and simulations was conducted with 156 plates scoping two different FRP materials, four different lay-ups, three different initial geometrical imperfections, and six or eight different laminate thicknesses. All plates were square, simply supported on four sides and with side dimensions of 500 mm. Both post-buckling strengths and ultimate compressive strengths were determined using a modelling methodology requiring both second-order nonlinear analysis and first-order linear analysis. 24 buckling curves were constructed and grouping the curves show correlations between the buckling reduction factor with slenderness. The parameter tending to be the most decisive in the variation of the buckling reduction factor is the type of lay-up in the

lamination. The choice of FRP material at ply level and/or magnitude of initial imperfection is found to have a lesser impact on post-buckling responses to ultimate failure.

Visually, there is a distinct difference between the six numerical-generated curves using results from the 36 unidirectional laminated plates and the other 18 curves comprising results from the 120 multi-directional laminated plates. A universal design buckling curve (and its formulae) is proposed by fitting a curve to the lower bound of the 18 buckling curves constructed from the analyses of the multi-directional plates. For a preliminary comparison, 45 experimental test results from four independent sources were used to benchmark the proposed buckling design curve. This important comparison reveals that the ABAQUS®-generated curve provides adequate predictions on the low side with acceptable reliability.

Using numerical results for ultimate failure and critical elastic buckling strengths (or loads) from the 120 multi-directional plates a lower-bound linear trendline formula is presented to predict a conservative ultimate failure load providing the user has knowledge of the critical elastic buckling load and plate slenderness.

The outcomes presented in this paper are based on a numerical parametric study, so to validate the new results (and the modelling methodology), there is a requirement for additional reliable and relevant experimental test results that scope the domain for FRP plate buckling. Furthermore, similar numerical analyses for post-buckling strengths of laminated plates need to be conducted with, for example, different types of loading and displacement boundary conditions to ensure that the proposed design buckling curve approach can be generalized with the potential of developing a universal set of curves. The goal of this research is to have recognized buckling curves that can appear in the Eurocode part that is to be prepared following the publication of the Technical Specification for *Design of Fibre-Polymer Composite Structures* (CEN/TS 19101:2022).

CRediT authorship contribution statement

Erik Olsson: Writing – original draft, Investigation, Formal analysis, Data curation. **J. Toby Mottram:** Writing – review & editing, Formal analysis. **Mohammad Al-Emrani:** Conceptualization. **Reza Haghani:** Writing – review & editing, Writing – original draft, Validation, Supervision, Resources, Project administration, Methodology, Formal analysis, Conceptualization.

Declaration of competing interest

The authors declare that they have no known competing financial interests or personal relationships that could have appeared to influence the work reported in this paper.

Data availability

No data was used for the research described in the article.

References

[1] V. Mara, R. Haghani, A. Sagemo, L. Stork, D. Nilsson, Comparative study of different bridge concepts based on life-cycle cost analyses and life-cycle assessment, in: Proceedings of the 4th Asia-Pacific Conference on FRP in Structures, APFIS 2013, 2013.

[2] M. Heshmati, R. Haghani, M. Al-Emrani, Environmental durability of adhesively bonded FRP/steel joints in civil engineering applications: State of the art, Composites B 81 (2015) 259–275.

[3] V. Mara, R. Haghani, P. Harryson, Bridge decks of fibre reinforced polymer (FRP): A sustainable solution, Constr. Build. Mater. 50 (2014) 190–199.

[4] V. Mara, M. Al-Emrani, R. Haghani, A novel connection for fibre reinforced polymer bridge decks: Conceptual design and experimental investigation, Compos. Struct. 117 (1) (2011) 83–97.

[5] V. Mara, R. Haghani, Review of FRP decks: Structural and in-service performance, Proc. Inst. Civ. Eng.: Bridge Eng. 168 (4) (2015) 308–329.

[6] R. Sonnenschein, K. Gajdosova, I. Holly, FRP composites and their using in the construction of bridges, Procedia Eng. 161 (2016) 447–482.

[7] A. Zyjeweski, L. Pyrzowski, The use of fiber-reinforced polymers (FRP) in bridges as favorable solution for the environment, E3S Web Conf. 17 (2017) 0012.

[8] J.T. Mottram, J. Henderson (Eds.), FRP Bridges – Guidance for Designers, CIRIA C779, London, 2018, https://tinyurl.com/yy79wl4b. [viewed 2022-11-14].

[9] R. Haghani, E. Olsson, FALCON - A multi-disciplinary effort to promote FRP bridges in Sweden, in: The 9th International Conference on Fibre-Reinforced Polymer (FRP) Composites in Civil Engineering, CICE 2018, 2018.

[10] T. Hara, Structural behaviour of FRP tunnel lining, Adv. Mater. Res. 831 (2013) 115–119.

[11] R. Haghani, J. Yang, M. Gutierrez, C.D. Eamon, J. Volz, Fiber reinforced polymer culvert bridges - A feasibility study from structural and LCC points of view, Infrastructures 6 (9) (2021) 128.

[12] Y. Shao, A. Peterson, FRP composite sheet pile walls for shoreline protection, in: Proceedings of the 33rd Canadian Society for Civil Engineering (CSCE) Annual Conference, 2005.

[13] CEN/TS 19101, Design of fiber-polymer composite structures, 2022, European Committee for Standardization, CEN/TC 250.

[14] A. André, M. Juntikka, C. Mattsson, G. Nedev, R. Haghani, The re-use of end-of-life fiber reinforced polymer composites in construction, in: The 10th International Conference on Fibre-Reinforced Polymer (FRP) Composites in Civil Engineering, CICE 2021, 2022, pp. 1183–1195, http://dx.doi.org/10.1007/978-3-030-88166-5_103.

[15] M. Pecce, E. Cosenza, Local buckling curves for the design of FRP profiles, Thin Walled Struct. 37 (2000) 207–222.

[16] G. Turvey, I.H. Marshall, Buckling and Postbuckling of Composite Plates, Springer Science, Dordrecht, 1995.

[17] K.A. Stevens, R. Ricci, G.A.O. Davies, Buckling and postbuckling of composite structures, Composites 26 (1995) 189–199.

[18] D.T. Borowitz, L.C. Bank, Web buckling in pultruded fiber-reinforced polymer deep beams subjected to concentrated loads, J. Compos. Constr. 18 (3) (2014) A4013014, 1-8.

[19] V. Mara, R. Haghani, M. Al-Emrani, Improving the performance of bolted joints in composite structures using metal inserts, J. Compo. Mater. 50 (2016) 3001–3018.

[20] A.S. Fallah, H.E. Johnson, L.A. Louca, Experimental and numerical investigation of buckling resistance of marine composite panels, J. Compos. Mater. 45 (8) (2011) 907–922.

[21] A.W. Leissa, Buckling of Laminated Composite Plates and Shell Panels, Flight Dynamics Laboratory Report No. AFWAL-TR-85-3069, The Ohio State University, Wright-Patterson Air Force Base, USA, 1985.

[22] U. Farooq, P. Myler, Finite element simulation of buckling-induced failure of carbon fibre-reinforced laminated composite panels embedded with damage zones, Acta Astronaut. 115 (2015) 314–329.

[23] S.G. Lekhnitskii, Anisotropic Plates, Gordon and Breach Science Publ, New York, 1968.

[24] J.M. Whitney, The effect of boundary conditions on the response of laminated composites, J. Compos. Mater. 4 (1970) 192–203.

[25] E. Gal, R. Levy, H. Abramovich, P. Pavsner, Buckling analysis of composite panels, Compos. Struct. 73 (2006) 179–185.

[26] A.K. Soh, L.C. Bian, J. Chakrabarty, Elastic/plastic buckling of a composite flat plate subjected to uniform edge compression, Thin-Walled Struct. 38 (2000) 247–265.

[27] D. Xie, S.B. Biggers Jr., Postbuckling analysis with progressive damage modelling in tailored laminated plates and shells with a cutout, Compos. Struct. 59 (2003) 199–216.

[28] L. Boni, D. Fanteria, A. Lanciotti, Post-buckling behaviour of flat stiffened composite panels: Experiments vs analysis, Compos. Struct. 94 (2012) 3421–3433.

[29] S.C. White, P.M. Weaver, K.C. Wu, Post-buckling analyses of variable-stiffness composite cylinders in axial compression, Compos. Struct. 123 (2015) 190–203.

[30] C. Bisagni, Numerical analysis and experimental correlation of composite shell buckling and post-buckling, Composites B 31 (8) (2000) 655–667.

[31] Q.J. Yang, B. Hayman, H. Osnes, Simplified buckling and ultimate strength analysis of composite plates in compression, Composites B 54 (1) (2013) 343–352.

[32] B.D. Agarwal, L.J. Broutman, K. Chandrashekhara, Analysis and Performance of Fiber Composites. [Electronic], fourth ed., John Wiley and Sons, Incorporated, Hoboken, USA, 2018.

[33] B. Hayman, C. Berggreen, C. Lundsgaard-Larsen, A. Delarche, H. Toftegaard, R.S. Dow, J. Downes, K. Misirlis, N. Tsouvalis, C. Douka, Studies of the buckling of composite plates in compression, Ships Offshore Struct. 6 (1–2) (2011) 81–92.

[34] Abaqus Documentation, Abaqus/CAE 2017, Dassault Systems Simula Corp, Johnston, RI, USA.

[35] Z. Hashin, Failure criteria for unidirectional composites, J. Appl. Mech. 47 (1980) 329–334.

[36] I. Lapczyk, J.A. Hurtado, Progressive Damage Modelling in Fiber-Reinforced Elements Subjected to In-Plane Compression, A Parametric Study on the Relation Between Slenderness and Buckling Reduction Factor (Master Thesis), Chalmers University of Technology, 2007.

[37] H.G. Johansson, E. Seebergs, Buckling and Post-Buckling Behaviours of Fibre Reinforced Elements Subjected to In-Plane Compression - A Parametric Study on the Relation Between Slenderness and Buckling Reduction Factor (Master Thesis), Chalmers University of Technology, 2018.
[38] Z. Hashin, A. Rotem, A fatigue failure criterion for fiber-reinforced materials, J. Compos. Mater. 7 (4) (1973) 448–464.
[39] N. Buskell, G.A.O. Davies, K.A. Stevens, Postbuckling failure of composite panels, Compos. Struct. 3 (1985) 290–314.
[40] G.B. Chai, W.M. Banks, J. Rhodes, An experimental study on laminated panels in compression, Compos. Struct. 19 (1991) 67–87.
[41] Ö. Namdar, H. Darendeliler, Buckling, postbuckling and progressive failure analyses of composite laminated plates under compressive loading, Composites B 120 (2017) 143–151.